RSC Advances

PAPER

View Article Online
View Journal | View Issue

Cite this: *RSC Adv.*, 2018, **8**, 32325

Chemical bond parameters, bond energy and the local crystal sites of Eu^{3+} in $Ca_5(BO_3)_3F$:1% Eu^{3+} phosphor

Yuhan Zhu, Yu Pan, Wenjun Wang, Haibing Xu, Liqun Zhou, Xiaoguang Liu* and Ling Li*

The local crystal sites occupied by Eu^{3+} in $Ca_5(BO_3)_3F$:1% Eu^{3+} phosphor were investigated experimentally and theoretically. $Ca_5(BO_3)_3F$:1% Eu^{3+} was synthesized by high-temperature solid-state method in air. The crystal structure and optical properties of the phosphor were studied by X-ray powder diffraction and photoluminescence, respectively. Two different $O^{2-} \rightarrow Eu^{3+}$ CT broad bands with the peaks at 266 and 283 nm in $Ca_5(BO_3)_3F$:1% Eu^{3+} were detected, indicating the Eu^{3+} sites occupied Ca2 and Ca1, respectively. The different sharp f–f emission spectra under the excitation of 283 and 266 nm proved that there are two different local lattice environments around Eu^{3+} existing in $Ca_5(BO_3)_3F$:1% Eu^{3+}. Environmental factor h_e, the standard deviation of environmental factor (EFSD) $\sigma(h_{e_i})$ and the bond energy were used to illustrate and explain the site occupancy mechanism of Eu^{3+} into the host lattice. By comparing the intensity ratios of $^5D_0 \rightarrow {}^7F_2$ transition to the $^5D_0 \rightarrow {}^7F_1$ transition, $I(^5D_0/^7F_2)/I(^5D_0/^7F_1)$ of Eu^{3+} at Ca2 (7.381) was found to be 2.5 times stronger than that of Eu^{3+} at Ca1 site (2.933). $\sigma(h_{e_i})$ was calculated to analyze the $I(^5D_0/^7F_2)/I(^5D_0/^7F_1)$ value. On the basis of the bond valence model, a bond-energy method was used to study the occupancy of the Eu ion, which indicated that the preferential sites of Eu ion occupancy in the $Ca_5(BO_3)_3F$ are the Ca2 and Ca1 sites. All three theoretical calculation results are consistent with each other.

Received 28th July 2018
Accepted 3rd September 2018

DOI: 10.1039/c8ra06357e

rsc.li/rsc-advances

1. Introduction

White LEDs have the advantages of high brightness, low energy consumption, long life, small size, no radiation, no pollution, *etc.* It is considered the new generation of green light sources. The two commonly used methods for implementing white LEDs are: blu-ray chip and YAG:Ce^{3+} yellow phosphor combination, and near-ultraviolet LED chip combined with the trichromatic phosphor. However, the former lacks the red portion, resulting in a lower color rendering index (less than 80) and a higher color temperature (greater than 40), while the latter is less commercially available and lacks suitable red light materials.[1–6] Therefore, finding a suitable red luminescent material and improving the color rendering index has become an important issue in the development of trichromatic white LEDs. In the rare earth family, Eu^{3+} ions are widely used in various fields of luminescent materials because they have good luminescence properties and can emit red fluorescence with good monochromaticity.[7–9] The luminescence of Eu^{3+} derived from the $4f^6$ transition consists of sharp peaks of the Eu^{3+}-doped inorganic compound in the red region.[10–12]

Rare earth ion-doped borate luminescent materials have high UV transparency, nonlinear characteristics, good stability and optical properties, and they are expected to become a promising fluorescent material, attracting more and more research worldwide.[13–15] Among the nonlinear optical crystal materials that have been found, ultraviolet and deep ultraviolet nonlinear optical crystals that have excellent performance are almost all borate compounds. $Ca_5(BO_3)_3F$ was first reported by Lei *et al.* in 1989. The crystal was also a new type of nonlinear optical crystal. The powder doubling effect was measured to be 2–3 KDP, and the transmission range was 190–3600 nm.[16,17] There are many published papers focusing on energy transfer and color-tunability of rare earth (*e.g.*, Bi^{3+}, Ce^{3+}, Tb^{3+})-doped $Ca_5(BO_3)_3F$.[18,19] There are three kinds of octahedrons surrounding the Ca ions that could be substituted by Eu^{3+}. They have different covalence, average bond lengths, central ion coordination numbers, and charges of ligands in chemical bonds. These result in Eu^{3+} ions with different photoluminescence properties. For the above reasons, $Ca_5(BO_3)_3F$ compound with Ca^{2+} and B^{3+} cationic sites can be selected as a host lattice, and Eu^{3+} ions are used as a good activator. However, studies on the effects of Eu^{3+} on the CT properties and

Hubei Collaborative Innovation Center for Advanced Organochemical Materials, Ministry-of-Education Key Laboratory for the Synthesis and Applications of Organic Functional Molecules, Hubei University, Wuhan, Hubei, China. E-mail: liling402431@hotmail.com; liuxiaoguang402@hotmail.com

the local crystal sites occupied by Eu^{3+} in $Ca_5(BO_3)_3F$:1% Eu^{3+} phosphor are rarely reported.

The environmental factor (h_e) was used to investigate the sites of Eu^{3+} based on the relationship between the CT bands of Eu^{3+} and the crystal structure of the host lattice. h_e can be calculated using the complex crystal chemical bond theory. The smaller the h_e, the larger the charge transfer energy from O^{2-} to Eu^{3+}. Through the literature, we know that the PL intensity ratio between the $^5D_0 \rightarrow {}^7F_2$ and $^5D_0 \rightarrow {}^7F_1$ transition of Eu^{3+} increases as the crystal distortion increases. The degree of distortion was calculated by the environmental factor standard deviation (EFSD) $\sigma(h_{e_i})$. This can provide information on the Eu ion sites. At the same time, the bond energy theory can be used to discuss the site occupancy of dopants into the host. In previous papers, this method has been proven; for example, the site preferential occupancy for Eu in $Sr_2V_2O_7$, $Sr_9Gd(VO_4)_7$ and $Sr_2V_2O_7/Sr_9Gd(VO_4)_7$, $CaAl_2Si_2O_8$ phosphors,[20] as well as Bi^{2+} in β-$Ca_2P_2O_7$ crystals,[21] have been solved though the bond energy method. Furthermore, this method was also used in study of bond energy and preferential occupancy of Eu^{3+} doped in the $Ca_{10}M(PO_4)_7$ (M = Li, Na, K) systems.[22]

In our work, Eu^{3+} doped $Ca_5(BO_3)_3F$ was prepared by a high-temperature solid-state method. We firstly used the chemical bond parameters and analyzed the sites of Eu ion systematically based on the refined crystal structure parameters. Then, the site occupancy of Eu^{3+} was investigated by analyzing the luminescent properties and environmental factor h_e and the standard deviation of environmental factor (EFSD) $\sigma(h_{e_i})$ of $Ca_5(BO_3)_3F$:1% Eu^{3+} when Eu^{3+} replaced the different Ca^{2+} sites in the matrix. Finally, the bond energy method was applied to illustrate and explain the site occupation of Eu^{3+} into the host lattice.

2. Experimental

2.1 Synthesis of material

$Ca_5(BO_3)_3F$:1% Eu^{3+} phosphor was prepared by high-temperature solid-state reaction in air. The desired CaF_2 (A.R., Macklin), H_3BO_3 (A.R., Sinopharm), $CaCO_3$ (99.99%, Aladdin), and Eu_2O_3 (99.99%, Aladdin) were weighed according to the stoichiometric ratio of $Ca_5(BO_3)_3F$:1% Eu^{3+}, and the raw materials were placed in an agate mortar and ground for half an hour. The uniformly mixed raw materials were transferred to an alumina crucible, heated in a crucible calciner to 1150 °C, and then kept for 4 h. After the sample was cooled to room temperature, it was ground into a powder to obtain the desired sample.

2.2 Material characterization

In this experiment, we used a Bruker D8 Advance X-ray diffractometer to analyze the crystal structure of the prepared phosphor with Cu Kα ($\lambda = 1.54056$ Å) radiation and acceleration voltage of 30 kV. The scanning range was 5 to 80 degrees. The sample was detected by FLS980 fluorescence spectrometer to obtain the excitation spectrum and emission spectrum. The excitation source was a 450 W Xe lamp with a slit width of 2 nm and a measured spectral range of 200 nm to 750 nm, with a resolution of 0.2 nm. The sample was tested at room temperature. The Rietveld structure refinement was performed using the General Structure Analysis System (GSAS)[23] software in order to determine the change of crystal structure.

3. Results and discussion

3.1 Phase characterization and crystal analysis

Fig. 1 is an XRD pattern of $Ca_5(BO_3)_3F$:1% Eu^{3+} sample. Comparing the sample diffraction pattern with the standard card, it was found that the diffraction peak data were basically consistent with the $Ca_5(BO_3)_3F$ (ICSD-65763) card data, with a $C1m1$ space group and a monoclinic crystal system. There is an impurity phase, namely, $Ca_3B_2O_6$. Fortunately, a very small amount of $Ca_3B_2O_6$ has no effect on our system. Therefore, the substitution of Eu^{3+} for Ca^{2+} into $Ca_5(BO_3)_3F$ did not change the structure of the crystal.

Fig. 2 shows the crystal structure of $Ca_5(BO_3)_3F$. There are three Ca ion coordination environments in this structure, namely, Ca1, Ca2 and Ca3. The anionic structural group of the $Ca_5(BO_3)_3F$ crystal is a planar BO_3 group. Both Ca and the surrounding anions form a CaO_4X_2 (X = F or O) octa-coordination, in which Ca(1) forms a CaO_5F octahedron with five O atoms and one F atom, and Ca(2) forms a distorted octahedral structure with six O atoms. Ca(3) is coordinated with two F atoms and four O atoms. These polyhedrons are connected to the BO_3 group by sharing O atoms to form a three-dimensional space structure.

The crystal structure of $Ca_5(BO_3)_3F$ (ICSD-65763) was used as the starting model for structure refinement. The Rietveld method refers to the point-by-point comparison of the calculated and measured values of the diffraction intensity of a crystal using a computer program, and the least squares method is used to adjust the parameters of the structural atoms and of the peak shape, so that the calculated peak shape is consistent with the measured peak shape. In the structural

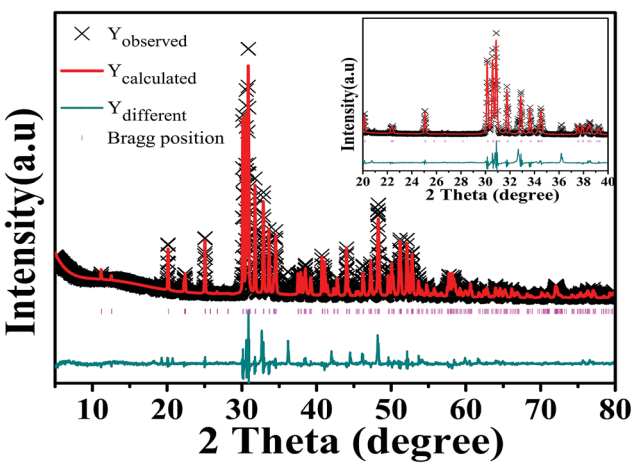

Fig. 1 Observed, calculated and difference X-ray diffraction patterns of an Eu^{3+} (1%)-doped $Ca_5(BO_3)_3F$ phosphor (the inset gives [20–40] 2θ range).

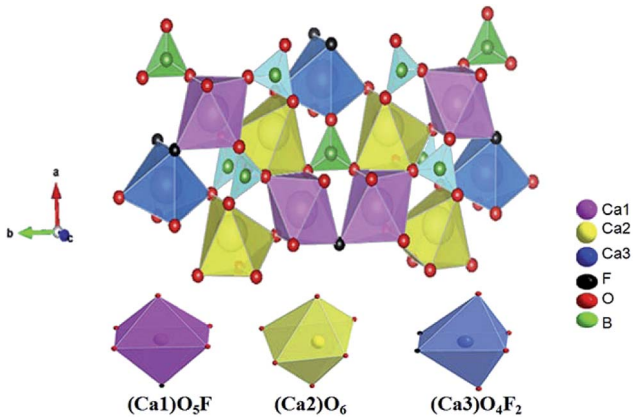

Fig. 2 Crystal structure of $Ca_5(BO_3)_3F$ and the coordination environment of Ca1, Ca2, and Ca3.

Table 1 Final crystallographic and refinement of parameter of $Ca_5(BO_3)_3F$:1% Eu^{3+}; *E* is the error between the original and refined value

Formula	$Ca_5(BO_3)_3F$	*E*
Space-group	*C*1*m*1	
a/Å	8.132	0.003
b/Å	16.054	0.003
c/Å	3.542	0.003
$\alpha = \gamma$	90°	0
β	100.946°	0
R_{wp}	5.30%	
R_p	9.35%	
χ^2	6.806	

refinement of this paper, based on the XRD peak of the existing $Ca_5(BO_3)_3F$:1% Eu^{3+} crystal and $Ca_5(BO_3)_3F$ standard card as the background, the set function is type 4, and about 30 terms were refined. Fig. 1 shows the observed, calculated and difference results for the Rietveld refinement of $Ca_5(BO_3)_3F$:1% Eu^{3+} phosphor. The peak intensities and positions exhibited few differences between the experimental and calculated patterns. Crystallographic and refinement parameters are summarized in Table 1. The results show that almost all diffraction peaks can be directed to $Ca_5(BO_3)_3F$ with a monoclinic unit cell (*C*1*m*1). The cell parameters *a*, *b*, *c*, and β, *etc.*, are close to those of $Ca_5(BO_3)_3F$ (ICSD-65763). The atomic coordinates and isotropic displacement parameters of $Ca_5(BO_3)_3F$:1% Eu^{3+} phosphor are listed in Table 2. The above results show that the crystal structure data of $Ca_5(BO_3)_3F$:1% Eu^{3+} simulated by refinement can be well matched with its experimental data.

3.2 Photoluminescence properties

Fig. 3(b) is an excitation spectrum of the $Ca_5(BO_3)_3F$:1% Eu^{3+} sample at a monitoring wavelength of 633 nm, which is composed of a broad excitation band of 225–350 nm, derived from the charge transfer transition of O^{2-} to Eu^{3+}, where the strongest absorption peak is at 266 nm. The emission spectrum at an excitation wavelength of 266 nm is shown in Fig. 3(d), consisting of emission peaks at around 576, 592, 612, 652 and 708 nm, corresponding to $^5D_0 \rightarrow {}^7F_0$, $^5D_0 \rightarrow {}^7F_1$, $^5D_0 \rightarrow {}^7F_2$, $^5D_0 \rightarrow {}^7F_3$, and $^5D_0 \rightarrow {}^7F_4$ transitions of Eu^{3+} ions, respectively.[24,25] We can clearly see that the charge transfer transition peaks of samples O to Eu have a significant shift when the monitoring wavelengths are 576, 612, 619 and 633 nm, as shown in Fig. 3(a) and (b). The two broadband peaks ($O^{2-} \rightarrow Eu^{3+}$) are located at 266 and 283 nm, respectively, which means that the Eu^{3+} ions exhibit two lattice environments in the $Ca_5(BO_3)_3F$ matrix. However, the excitation and emission spectra of Eu-doped $Ca_3B_2O_6$ are completely different with our luminescence properties of Eu-doped $Ca_5(BO_3)_3F$. The former shows an emission band peaking at 422 nm and excitation peaks at 362, 380 and 394 nm (λ_{em} = 616 nm). These prove that the different luminescence of Eu is due to Eu occupying the different sites in the $Ca_5(BO_3)_3F$.[26]

When the Eu^{3+} ion deviates from the center of the inversion, due to the opposite parity configuration in the 4f configuration, the parity selection in the crystal is relaxed and the $^5D_0 \rightarrow {}^7F_2$ electric dipole transition will occur. If the Eu^{3+} ion is located in the non-inversion center, its emission spectrum will be dominated by the $^5D_0 \rightarrow {}^7F_2$ electric dipole transition, and the emission spectrum will be around 610 nm. For the electronic transition of Eu^{3+} ion, the $^5D_0 \rightarrow {}^7F_0$ transition originally belongs to the forbidden transition. However, when it is in the ten symmetry positions of C_s, C_1, C_2, C_3, C_4, C_6, C_{2v}, C_{3v}, C_{4v} and C_{6v}, $^5D_0 \rightarrow {}^7F_0$ transition emission will occur, and the emission

Table 2 Atomic coordinates and isotropic displacement parameters (U_{iso}/Å^2) for $Ca_5(BO_3)_3F$:1% Eu^{3+}; *E* is the error between the original and refined value

Name	*x*	*y*	*z*	$E_{position}$	Mult	Occ	U_{iso}	$E_{U_{iso}}$
Ca1	0.6501	0.1177	0.7786	0.013	4	1	0.0231	0.001
Ca2	0.0278	0.1796	0.4421	0.02	4	1	0.0145	0.002
Ca3	0.2583	0	0.0769	0.04	2	1	0.0283	0.02
F1	0.4691	0	−0.3287	0.03	2	1	0.0737	0.01
O1	0.8282	0.0743	0.3639	0.01	4	1	0.0603	0.002
O2	−0.001	0.3279	0.2448	0.018	4	1	0.0504	0.001
O3	0.0722	0	0.5116	0.024	2	1	0.0066	0.002
O4	0.829	0.2254	0.8459	0.049	4	1	0.0307	0.02
O5	0.2071	0.143	0.0125	0.02	4	1	0.0134	0.001
B1	0.8626	0.307	0.0036	0.014	4	1	0.0594	0.011
B2	0.9239	0	0.3499	0.006	2	1	−0.0113	0.003

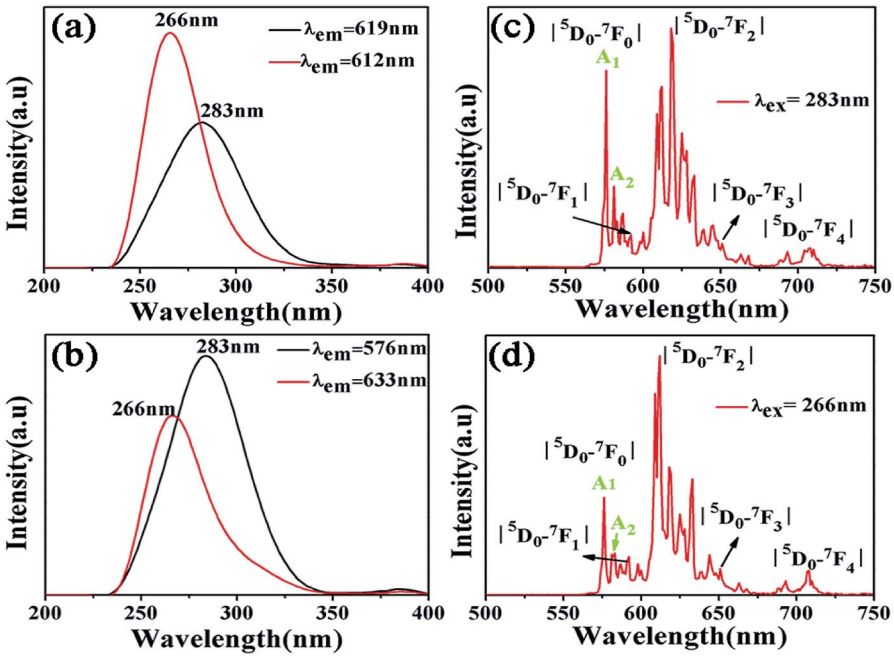

Fig. 3 (a) and (b) Excitation spectra under different monitoring wavelengths of $Ca_5(BO_3)_3F$:1% Eu^{3+}; (c) and (d) emission spectra of $Ca_5(BO_3)_3F$:1% Eu^{3+} under 266 and 283 nm excitation.

spectrum peak will be around 580 nm. A $^5D_0 \rightarrow {}^7F_0$ transition peak appears in each site.[27] Therefore, based on the number of the peaks, the number of occupied sites of the Eu^{3+} ion crystals can be judged. Fig. 3(c) and (d) show the emission spectra of $Ca_5(BO_3)_3F$:1% Eu^{3+} upon excitation at 266 nm and 283 nm, respectively. Their peaks locate at 576 nm, which is due to $^5D_0 \rightarrow {}^7F_0$ transition of Eu^{3+} ions. Each $^5D_0 \rightarrow {}^7F_0$ transition peak corresponds to a lattice. Two $^5D_0 \rightarrow {}^7F_0$ peaks, A_1 and A_2, were found in Fig. 3(c) and (d), which indicate that Eu^{3+} doping in $Ca_5(BO_3)_3F$ has two sites.[28–30] The data are shown in Table 3 for the luminescent levels of $Ca_5(BO_3)_3F$:1% Eu^{3+} upon 266 and 283 nm excitation.

Since CT energy is susceptible to the central ionic environment, it can be quantitatively expressed by using environmental factors (h_e). h_e consists of four chemical bond parameters: the bond volume polarization ($\alpha_b{}^\mu$), the covalency ($f_c{}^\mu$), the coordination number (C. N.) and the presented charge of the ligand ($Q_B{}^\mu$). Its calculation formula is as follows:[31]

$$h_e = \left(\sum_\mu f_c{}^\mu \alpha_b{}^\mu Q_B{}^{\mu 2} \right)^{1/2} \quad (1)$$

where $f_c{}^\mu$ represents the covalent value of μ type bond, $Q_B{}^\mu$ is the charge exhibited by the nearest anion and $\alpha_b{}^\mu$ stands for the polarizability of the μ-type chemical bond volume.

The four chemical bond parameters, with any change, will cause a shift in the CT bands. As h_e increases, the CT energy decreases, which means that the CT bands will produce a red shift. In Table 4, we can see that the h_e values of Ca1, Ca2, and Ca3 are 0.6397, 0.7439, and 0.3514, respectively. Therefore, it can be known that Eu will occupy the Ca1 and Ca2 sites, and at the same time, the O–Eu1 CT band at the Ca1 site corresponds to the peak at 266 nm and the O–Eu2 CT band at Ca2 corresponds to the position at 283 nm.

Obviously, the intensity of f–f transitions is affected by the crystal environment because of the different symmetry of the doping ions occupying the host sites. When the Eu^{3+} is doped into $Ca_5(BO_3)_3F$, the Eu ions occupy the Ca^{2+} sites, wherefore,

Table 3 The data for the luminescent levels of $Ca_5(BO_3)_3F$:1% Eu^{3+} upon 266 and 283 nm excitation

Energy level transition	The location of the peak (nm) (λ_{ex} = 266 nm)	Intensity	The location of the peak (nm) (λ_{ex} = 283 nm)	Intensity
$^5D_0 \rightarrow {}^7F_0$	576		576	
	583		581	
$^5D_0 \rightarrow {}^7F_1$	592	233 668.172	592	149 367.984
$^5D_0 \rightarrow {}^7F_2$	612	685 254.813	618	1 102 500
$^5D_0 \rightarrow {}^7F_3$	652		651	
$^5D_0 \rightarrow {}^7F_4$	708		708	
$\frac{^5D_0 \rightarrow {}^7F_2}{^5D_0 \rightarrow {}^7F_1}$		2.933		7.381

Table 4 The chemical bond parameters, environmental factor h_e, the experimental $O^2 \rightarrow Eu^{3+}$ charge transfer band, the environmental factor of any individual bond (h_{e_i}) and their standard deviation of the Ca–O environmental factors$\sigma(h_{e_i})$

Central ion	Bond type	Distance (Å)	f_c^{μ}	α_b^{μ}	Q_B^{μ}	C.N.	h_e	(h_{e_i})	$\sigma(h_{e_i})$	O–Eu charge transfer peak
Ca1/Eu	Ca1–O1	2.3556	0.1160	0.4491	1.3333	1	0.6397	0.3043	0.1607	266 nm
	Ca1–O1	2.3960	0.1151	0.4819	1.3333	1		0.3140		
	Ca1–O2	2.2283	0.1191	0.3569	1.3333	1		0.2748		
	Ca1–O2	2.4020	0.1150	0.4870	1.3333	1		0.3155		
	Ca1–O4	2.2428	0.1187	0.3666	1.3333	1		0.2781		
	Ca1–F	2.3810	0.0258	0.2053	1.3333	1		0.0970		
Ca2/Eu	Ca2–O1	2.3237	0.1167	0.4244	1.3333	1	0.7439	0.2967	0.0184	283 nm
	Ca2–O2	2.4795	0.1135	0.5557	1.3333	1		0.3348		
	Ca2–O4	2.4653	0.1137	0.5426	1.3333	1		0.3312		
	Ca2–O4	2.5136	0.1129	0.5882	1.3333	1		0.3436		
	Ca2–O5	2.3311	0.1165	0.4300	1.3333	1		0.2984		
	Ca2–O5	2.3726	0.1156	0.4627	1.3333	1		0.3083		
Ca3/Eu	Ca3–O3	2.2691	0.1050	0.3493	1.0000	1	0.3514	0.1915	0.0520	
	Ca3–O3	2.3551	0.1031	0.4080	1.0000	1		0.2051		
	Ca3–O5	2.3363	0.1056	0.2512	0.6667	1		0.1086		
	Ca3–O5	2.3371	0.1056	0.2515	1.0000	1		0.1630		
	Ca3–F	2.4366	0.0257	0.2289	1.0000	1		0.0767		
	Ca3–F	2.4497	0.0257	0.2347	1.0000	1		0.0777		

the f–f transition relative intensity is mainly affected by the Ca^{2+} symmetry. The different $^5D_0 \rightarrow {}^7F_J$ transition intensities of Eu^{3+} depend on the local symmetry of the Eu^{3+} ion crystal field. The $^5D_0 \rightarrow {}^7F_2$ transition is sensitive, while the $^5D_0 \rightarrow {}^7F_1$ transition is stable to the crystal field environment. For example, when the Eu^{3+} ion is in a site with a strict inversion center, it will be dominated by the allowable $^5D_0 \rightarrow {}^7F_1$ magnetic dipole transition, and the emission spectrum is around 590 nm, which is orange light. When the Eu^{3+} ion is in the site away from the inversion center, the parity selection in the crystal is relaxed, and a $^5D_0 \rightarrow {}^7F_2$ electric dipole transition will occur; the emission spectrum is around 610 nm, emitting red light. If the intensity of the $^5D_0 \rightarrow {}^7F_2$ transition is much higher than the intensity of $^5D_0 \rightarrow {}^7F_1$, the Eu^{3+} ion mainly occupies the non-inversion symmetry of the lattice. It is known that the PL intensity ratio between $^5D_0 \rightarrow {}^7F_2$ and $^5D_0 \rightarrow {}^7F_1$ transition of Eu^{3+} increases as the crystal distortion increases. The degree of distortion can be calculated by using the standard deviation of

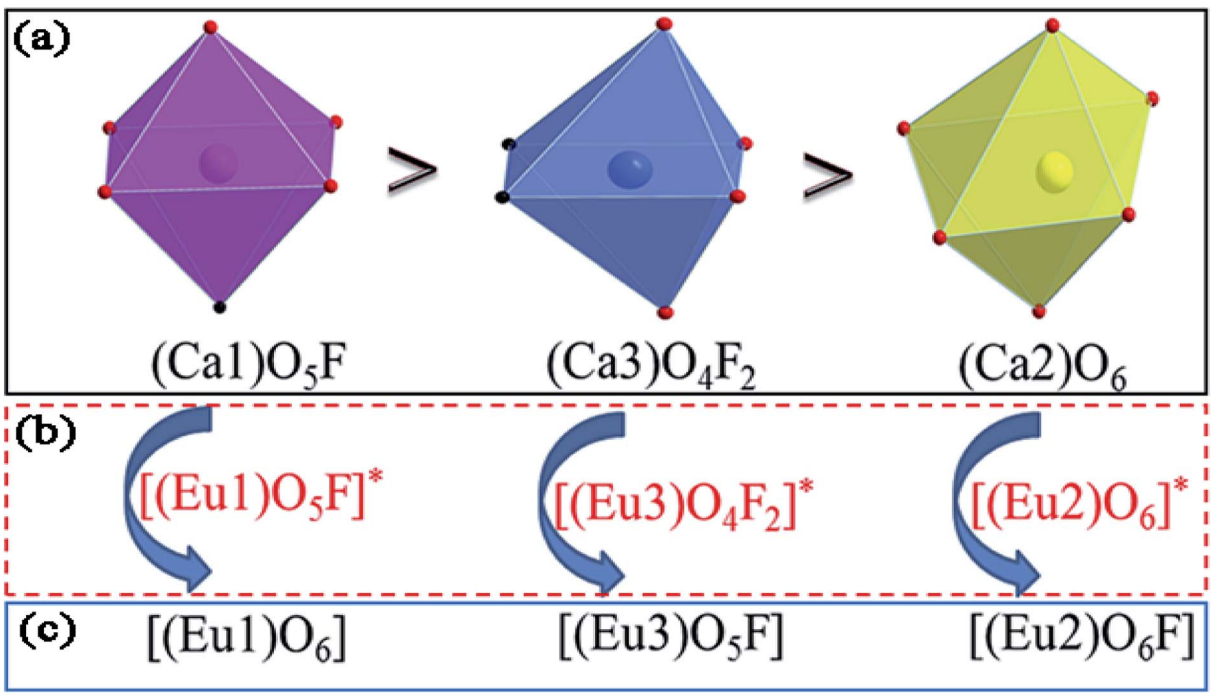

Fig. 4 The coordination environment mechanism of Ca1 (or Eu1), Ca2 (or Eu2), and Ca3 (or Eu3) in $Ca_5(BO_3)_3F$:1% Eu.

Table 5 Required d_0 and J values

Ions	d_0 (Å)	J (kcal mol^{-1})
Ca^{2+}–O^{2-}	1.967	126.60
Ca^{2+}–F^{-}	1.842	187.03
B^{3+}–O^{2-}	1.371	126.30
Eu^{3+}–F^{-}	2.056	163.35
Eu^{3+}–O^{2-}	2.074	109.40

environmental factor (EFSD)$\sigma(h_{e_i})$,[22,32] which can be calculated as below:

$$\sigma(h_{e_i}) = \sqrt{\frac{1}{N}\sum_{i=1}^{N}(h_{e_i} - \delta)^2} \quad (2)$$

where

$$h_{e_i} = \left(f_c^{\mu}\alpha_b^{\mu}\right)^{1/2} Q_B^{\mu} \quad (3)$$

and

$$\delta = \frac{1}{N}\sum_{i=1}^{N} h_{e_i} \quad (4)$$

The related chemical parameters of the covalency f_c^{μ}, the present charge of the ligand in the binary crystals, and the polarizability of the chemical bond volume α_b^{μ} are shown in Table 4. On the basis of the eqn (2)–(4), their standard deviation for the six Ca–O environmental factors $(\sigma(h_{e_i}))$ of $Ca1O_5F$, $Ca2O_4F_2$, and $Ca3O_6$ polyhedrons in $Ca_5(BO_3)_3F$:1% Eu can be calculated to be 0.1607, 0.0184 and 0.052, respectively. Generally, the $I(^5D_0/^7F_2)/I(^5D_0/^7F_1)$ value of Eu^{3+} increases with increasing $\sigma(h_{e_i})$. The $\sigma(h_{e_i})$ value of $Ca1O_5F$ in $Ca_5(BO_3)_3F$:1% Eu is larger than that of $Ca2O_4F_2$. By comparison, the intensity ratio of $^5D_0 \rightarrow {}^7F_2$ transition to the $^5D_0 \rightarrow {}^7F_1$ transition of Eu^{3+} at Ca2 (7.381) is 2.5 times stronger than that of Eu^{3+} at Ca1 site (2.933). Therefore, the $I(^5D_0 \rightarrow {}^7F_2)/I(^5D_0 \rightarrow {}^7F_1)$ of Eu^{3+} in the $Ca1O_5F$ site is stronger than that in the $Ca2O_4F_2$ site. Ca1 and Ca2 correspond to excitations at 283 nm and 266 nm, respectively. However, this is contrary to the conclusion drawn in Table 4. In ideal state, the order of $\sigma(h_{e_i})$ is in Fig. 4. When Eu^{3+} is doped into $Ca_5(BO_3)_3F$, part of the Ca^{2+} ions must be occupied by Eu^{3+}, so the local environment of Eu^{3+} must be changed in order to keep the conservation of charge in Fig. 4(a) and (b). At this time, one F of the substationary [(Eu1)O_5F]* and [(Eu3)O_4F_2]* will be replaced by an O to maintain their own stability; [(Eu2)O_6]* will receive an F, and it will eventually become a 7-coordinated environment in Fig. 4(c). In summary, we can conclude that the Ca2 distortion degree should be greater than that of Ca1. Therefore, Ca1 and Ca2 correspond to excitations at 266 nm and 283 nm, respectively, consistent with the results obtained in Table 4.

3.3 Chemical bond energy calculation

From the point of view of matched valence, the bond energy of Eu^{3+} into the $Ca_5(BO_3)_3F$ phosphor can be estimated by the following equation,[20,33]

Table 6 The bond parameters of the central atom and values of bond energy when Eu^{3+} locates at Ca and B sites in $Ca_5(BO_3)_3F$. All of the bond energy units are kcal mol^{-1}

Central atom	Coordination atom	Count	d (Å)	E_{M-O}	$E^{M}_{Eu^{3+}-O^{2-}}$	$\Delta E^{M}_{Eu^{3+}-O^{2-}}$
Ca1	O2	1×	2.2283	62.4781	48.0633	11.0351
	O4	1×	2.2428	60.0770	46.2162	
	O1	1×	2.3556	44.2901	34.0716	
	O1	1×	2.3960	39.7088	30.5473	
	O2	1×	2.4020	39.0701	30.0559	
	F1	1×	2.3810	41.3517	31.8111	
Ca2	O1	1×	2.3237	48.2781	48.0632	1.7744
	O2	1×	2.4795	31.6867	46.2162	
	O4	1×	2.4653	32.9264	34.0716	
	O4	1×	2.5136	28.8969	30.5473	
	O5	1×	2.3311	47.3221	30.0559	
	O5	1×	2.3726	42.3012	31.8111	
Ca3	O3	1×	2.2691	55.9549	37.1394	14.2389
	O3	1×	2.3551	44.3500	24.3760	
	O5	1×	2.3363	46.6617	25.3297	
	O5	1×	2.3371	46.5609	22.2299	
	F1	1×	2.4366	35.5821	36.4041	
	F1	1×	2.4497	34.3444	32.5416	
B1	O4	1×	1.4296	107.8004	734.209	551.7228
	O5	1×	1.5032	88.35499	707.712	
	O2	1×	1.3091	149.2999	687.725	
B2	O1	1×	1.4297	107.7712	624.1322	636.8898
	O1	1×	1.4304	107.5676	622.9525	
	O3	1×	1.2329	183.4429	1062.3664	

$$E_{M-O} = J \exp\left(\frac{d_0 - d_{M-O}}{0.37}\right)\left(\frac{V_N}{V_M}\right) \quad (5)$$

where V_M presents the dopant valence and V_N stands for the valence state of N. When the pure $Ca_5(BO_3)_3F$ phosphor does not have any dopant, the value of V_N/V_M is 1. This indicates that the valence state has no effect on the bond energy. If V_N/V_M is not equal to 1, it implies that the valence state effectively affects the crystal bond energy. Consequently, the effect of different valence states of the dopant on the Ca^{2+} site bond energy can be quantitatively described through eqn (5). The J and d_0 values are given in the report of Li;[34] d_{M-O} represents the bond length between atoms M and O. Required d_0 and J value tables are in Table 5. When Eu enters $Ca_5(BO_3)_3F$, the bond energy difference is calculated by the following equation:

$$\Delta E^{Eu}_{M-O} = |E_{M-O} - E_{Eu-O}| \quad (6)$$

Here, ΔE^{Eu}_{M-O} is the bond energy difference when the Eu ion locates at the site of Ca^{2+}. As previously reported, we can know that the dopants preferentially occupy a site where the bond energy difference is small (ΔE^{Eu}_{M-O}), that is, a site having a smaller absolute value of ΔE^{Eu}_{M-O}.[20]

According to the detailed crystallographic data from a pure $Ca_5(BO_3)_3F$ phosphor (longer Ca–O bonds of 1.967 Å; shorter B–O bonds of 1.371 Å; longer Ca–F bonds of 1.842 Å), all calculated E_{M-O} and ΔE_{M-O} values of Eu^{3+} on both Ca^{2+} and B^{3+} sites are shown in Table 6. The corresponding occupancies of Eu^{3+} are summarized, according to the calculated ΔE^{M}_{M-O} values. Dopants preferentially occupy the sites where the bond energy difference (ΔE^{M}_{M-O}) is smaller; that is, Eu^{3+} ions preferentially occupy Ca^{2+} sites if $|\Delta E^{Ca}_{Eu-O}| < |\Delta E^{B}_{Eu-O}|$; they preferentially occupy B^{3+} sites if $|\Delta E^{Ca}_{Eu-O}| > |\Delta E^{B}_{Eu-O}|$, otherwise.

There are three Ca^{2+} sites and two B^{3+} sites in the structure of $Ca_5(BO_3)_3F$. On the basis of the bond energy method, the values of ΔE^{Ca}_{Eu-O} and ΔE^{B}_{Eu-O} have been listed in Table 6. The order of difference of bond energy that $Ca^{2+}$and B^{3+} ions are replaced by Eu^{3+} is $\Delta E^{Ca2}_{Eu-O} < \Delta E^{Ca1}_{Eu-O} < \Delta E^{Ca3}_{Eu-O} \ll \Delta E^{B1}_{Eu-O} < \Delta E^{B2}_{Eu-O}$, which means that Eu^{3+} preferentially replaces Ca2 and Ca1. According to our calculation, Eu^{3+} preferentially occupies Ca2 and Ca1 sites, which is consistent with the environmental factor, the $\sigma(h_{e_i})$ analysis and PL spectrum.

4. Conclusions

The photoluminescence of $Ca_5(BO_3)_3F$:1% Eu^{3+} shows that the excitation spectrum consists of some broadband from the $O^{2-} \rightarrow Eu^{3+}$ charge transfer (CT) band and some sharp emission peaks derived from the f–f transition of Eu^{3+}. Two different $O^{2-} \rightarrow Eu^{3+}$ CT broad bands with the peaks at 266 and 283 nm in $Ca_5(BO_3)_3F$:1% Eu^{3+} can be assigned to the Eu^{3+} sites occupying Ca1 and Ca2, respectively. Two $^5D_0 \rightarrow {}^7F_0$ peaks, A_1 and A_2, were found, which implies that Eu^{3+} doped in $Ca_5(BO_3)_3F$ has two sites. According to the dielectric theory of the crystal, the important chemical bonds such as the polarizability, the covalency and the environmental factor were quantitatively calculated. When Eu^{3+} ions occupy the Ca1, Ca2 and Ca3 sites of $Ca_5(BO_3)_3F$, their environmental factors are 0.6397, 0.7439 and 0.3514, respectively. The intensity ratio of $^5D_0 \rightarrow {}^7F_2$ transition to the $5D_0 \rightarrow 7F_1$ transition of Eu^{3+} at Ca2 (7.381) is 2.5 times stronger than that of Eu^{3+} at Ca1 site (2.933). The calculated ideal $\sigma(h_{e_i})$ showed that the $I(^5D_0/^7F_2)/I(^5D_0/^7F_1)$ value at Eu1 is larger than that at Eu2 site. The local nonequivalence substitution distortion model was proposed to explain the result. The smaller deviation value of the bond energy method of ΔE^{Ca2}_{Eu-O} and ΔE^{Ca1}_{Eu-O} showed that the preferential sites of Eu^{3+} ion occupancy in $Ca_5(BO_3)_3F$ are Ca2 and Ca1. All of results are consistent with each other. The three theoretical methods provide us a new strategy to study the occupancy of Eu^{3+} in Eu^{3+}-doped inorganic compounds.

Conflicts of interest

There are no conflicts to declare.

Acknowledgements

This work is financially supported by the National Natural Science Foundations of China (Grant no. 21301053 and 21571165) and Hubei Natural Science Foundations from Science and Technology Department of Hubei Province (2018CFB517).

Notes and references

1 D. Liu, Y. Jin, Y. Lv, G. Ju, C. Wang, L. Chen, W. Luo and Y. Hu, *J. Am. Ceram. Soc.*, 2018, DOI: 10.1111/jace.15877, ahead of print.
2 H.-W. Wei, X.-M. Wang, H. Jiao and X.-P. Jing, *J. Alloys Compd.*, 2017, **726**, 22–29.
3 H. Xu, L. Wang, L. Tan, D. Wang, C. Wang and J. Shi, *J. Am. Ceram. Soc.*, 2018, **101**, 3414–3423.
4 R. Wei, L. Wang, F. Hu, X. Li, X. Peng, Y. Shi, H. Guo and J. Qiu, *J. Lumin.*, 2018, **197**, 291–296.
5 A. K. Pal, S. Som and C.-H. Lu, *Ceram. Int.*, 2018, **44**, 18256–18263.
6 Y. Miao, K. Wang, L. Gao, B. Zhao, H. Wang, F. Zhu, B. Xu and D. Ma, *J. Mater. Chem. C*, 2018, **6**, 8122–8134.
7 P. Chen, D. Yang, W. Hu, J. Zhang and Y. Wu, *Chem. Phys. Lett.*, 2017, **689**, 169–173.
8 Z. Xie, W. Zhou, W. Zhao, H. Zhang, Q. Hu and X. Xu, *Chem. Phys. Lett.*, 2017, **685**, 177–184.
9 T. S. Sreena, P. P. Rao, A. K. V. Raj and T. R. A. Thara, *J. Alloys Compd.*, 2018, **751**, 148–158.
10 G. Li, Y. Wei, W. Long and G. Xu, *Mater. Res. Bull.*, 2017, **95**, 86–94.
11 A. Kruopyte, R. Giraitis, R. Juskenas, D. Enseling, T. Justel and A. Katelnikovas, *J. Lumin.*, 2017, **192**, 520–526.
12 D. Kumar, B. P. Singh, M. Srivastava, A. Srivastava, P. singh, A. Srivastava and S. K. Srivastava, *J. Lumin.*, 2018, **203**, 507–514.
13 K. Das, A. Marathe, X. Zhang, Z. Zhao and J. Chaudhuri, *RSC Adv.*, 2016, **6**, 95055–95061.

14 A. Huang, Z. Yang, C. Yu, Z. Chai, J. Qiu and Z. Song, *Mater. Lett.*, 2016, **185**, 440–442.
15 P. Chen, F. Mo, A. Guan, R. Wang, G. Wang, S. Xia and L. Zhou, *Appl. Radiat. Isot.*, 2016, **108**, 148–153.
16 G. Chen, Y. Wu and P. Fu, *J. Cryst. Growth*, 2006, **292**, 449–453.
17 N. Kozhaya, M. Ferriol, M. Cochez, M. Aillerie and A. Maillard, *Opt. Mater.*, 2011, **33**, 1621–1625.
18 X. Li, P. Li, Z. Wang, S. Liu, Q. Bao, X. Meng, K. Qiu, Y. Li, Z. Li and Z. Yang, *Chem. Mater.*, 2017, **29**, 8792–8803.
19 L. Yi, J. Zhang, Z. Qiu, W. Zhou, L. Yu and S. Lian, *RSC Adv.*, 2015, **5**, 67125–67133.
20 L. Li, W. Wang, Y. Pan, Y. Zhu, X. Liu, H. M. Noh, B. K. Moon, B. C. Choi and J. H. Jeong, *RSC Adv.*, 2018, **8**, 1191–1202.
21 L. Li, J. Cao, B. Viana, S. Xu and M. Peng, *Inorg. Chem.*, 2017, **56**, 6499–6506.
22 W. Wang, Y. Pan, Y. Zhu, H. Xu, L. Zhou, X. Liu, L. Li, H. M. Noh and J. H. Jeong, *Dalton Trans.*, 2018, **47**, 6507–6518.
23 B. H. Toby, *J. Appl. Crystallogr.*, 2001, **34**, 210–213.
24 Y. Zhang, A. Abraha, R. Zhang, T. Shahbazyan, M. Fadavi, E. Heydari and Q. Dai, *Opt. Mater.*, 2018, **84**, 115–122.
25 W. You, Z. Xiao, F. Lai, X. Ye, C. Wang and H. Jiang, *Zhongguo Xitu Xuebao*, 2016, **34**, 11–16.
26 M. Shi, C. Zhu, M. Lu, X. Meng and M. Wei, *J. Am. Ceram. Soc.*, 2018, DOI: 10.1111/jace.15782, ahead of print.
27 J. B. Gruber, U. Vetter, T. Taniguchi, G. W. Burdick, H. Hofsaess, S. Chandra and D. K. Sardar, *J. Appl. Phys.*, 2011, **110**, 023104.
28 L. Zhou, J. Shi and M. Gong, *J. Lumin.*, 2005, **113**, 285–290.
29 P. A. Tanner, Y. Y. Yeung and L. Ning, *J. Phys. Chem. A*, 2013, **117**, 2771–2781.
30 Y. Zhang, Q. Xiao, H. He, J. Zhang, G. Dong, J. Han and J. Qiu, *J. Mater. Chem. C*, 2015, **3**, 10140–10145.
31 L. Li, X. Liu, H. M. Noh, S. H. Park, J. H. Jeong and K. H. Kim, *J. Alloys Compd.*, 2015, **620**, 324–328.
32 L. Li, Y. Pan, W. Wang, W. Zhang, Z. Wen, X. Leng, Q. Wang, L. Zhou, H. Xu, Q. Xia, L. Liu, H. Xiang and X. Liu, *J. Alloys Compd.*, 2017, **726**, 121–131.
33 Y. He and D. Xue, *J. Phys. Chem. C*, 2007, **111**, 13238–13243.
34 L. Li, Y. Pan, W. Wang, Y. Zhu, W. Zhang, H. Xu, L. Zhou and X. Liu, *J. Alloys Compd.*, 2018, **731**, 496–503.